Lo Wei-Ching (Orcid ID: 0000-0002-1893-0500)
Kayat Bittencourt Leonardo (Orcid ID: 0000-0001-9175-9626)
Jiang Yun (Orcid ID: 0000-0002-0713-9641)

Running Title: Multicenter Repeatability and Reproducibility of MR Fingerprinting in Phantoms and in Prostatic Tissue

Multicenter Repeatability and Reproducibility of MR Fingerprinting in Phantoms and in Prostatic Tissue

Wei-Ching Lo[1,2], Leonardo Kayat Bittencourt[3,4], Ananya Panda[5], Yun Jiang[6], Junichi Tokuda[7,8], Ravi Seethamraju[2], Clare Tempany-Afdhal[7,8], Verena Obmann[9], Katherine Wright[6], Mark Griswold[1,3], Nicole Seiberlich[6], Vikas Gulani[6]

[1]Dept. of Biomedical Engineering, Case Western Reserve University, Cleveland, OH, United States.
[2]Siemens Medical Solutions Inc., Boston, MA, United States
[3]Dept. of Radiology, University Hospital and Case Western Reserve University, Cleveland, OH, United States.
[4]DASA company, Rio de Janeiro, RJ, Brazil.
[5]Dept. of Radiology, Mayo Clinic, Rochester, MN, United States.
[6]Dept. of Radiology, University of Michigan, Ann Arbor, MI, United States.
[7]Dept. of Radiology, Harvard Medical School, Harvard University, Boston, MA, United States.
[8]Dept. of Radiology, Brigham and Women's Hospital, Boston, MA, United States.
[9]Dept. of Diagnostic, Interventional and Pediatric Radiology, Inselspital Bern, University of Bern, Berne, Switzerland

---

Corresponding author:

Vikas Gulani, MD, PhD

Department of Radiology, University of Michigan

University of Michigan Health System

1500 E. Medical Center Drive

Ann Arbor, Michigan 48109-5030

(E-mail: vikasgulani@med.umich.edu)

Submit to MRM as Technical Note (up to 2800 words, 5 figures plus tables)

Manuscript Word Count: 2839

Abstract Word Count: 250

Figures: 4 (+3 Supporting Information)

Tables: 1

ABSTRACT

Purpose

To evaluate multicenter repeatability and reproducibility of T_1 and T_2 maps generated using Magnetic Resonance Fingerprinting (MRF) in the ISMRM/NIST MRI system phantom and in prostatic tissues.

Methods

MRF experiments were performed on five different 3T MRI scanners at three different institutions: University Hospitals Cleveland Medical Center, Brigham and Women's Hospital in the United States, and Diagnosticos da America in Brazil. Raw MRF data were reconstructed using a Gadgetron-based MRF online reconstruction pipeline to yield quantitative T_1 and T_2 maps. The repeatability of T_1 and T_2 values over six measurements in the ISMRM/NIST MRI system phantom was assessed to demonstrate intra-scanner variation. The reproducibility between the four clinical scanners was assessed to demonstrate inter-scanner variation. The same-day test-retest normal prostate mean T_1 and T_2 values from peripheral zone and transitional zone were also compared using the intra-class correlation coefficient and Bland-Altman analysis.

Results

The intra-scanner variation of values measured using MRF was less than 2% for T_1 and 4.7% for T_2 for relaxation values within the range of 307.7 to 2360ms for T_1 and 19.1 to 248.5ms for T_2. Inter-scanner measurements showed that the T_1 variation was less than 4.9% and T_2 variation was less than 8.1% between multicenter scanners. Both T_1 and T_2 values in *in-vivo* prostatic tissue demonstrated high test-retest reliability (ICC > 0.92) and strong linear correlation (R^2 > 0.840).

Conclusion

Prostate MRF measurements of T_1 and T_2 are repeatable and reproducible between MRI scanners at different centers on different continents, for the above measurement ranges.

Key Words: prostate; MR fingerprinting; quantitative imaging; repeatability; reproducibility

INTRODUCTION

Magnetic Resonance Fingerprinting (MRF) (1) is a quantitative tissue property mapping technique that can be used to efficiently generate multiple tissue property maps simultaneously (2–6), and has been applied to measure quantitative T_1 and T_2 measurements in the prostate (2,7,8). MRF has the potential to enable objective diagnosis and follow-up of disease in the prostate. Previous research has shown that MRF-derived T_1 and T_2 values can be used to differentiate between normal peripheral zone (PZ) and prostate cancer (2,9,10), and in combination with apparent diffusion coefficient mapping can differentiate between low and intermediate/high grade cancers (7,11). MRF-based relaxometry combined with ADC mapping also improves transition zone (TZ) lesion characterization (8,12).

In order to translate and use MRF meaningfully in clinical practice, the quantitative tissue properties measured with MRF must be repeatable and reproducible (13). If these features can be demonstrated, observed relaxation time differences within a tissue can be assumed to be due to differences in physiology rather than measurement variability and/or scanner instability, as long as the measured differences are greater than the measurement error. MRF has been shown to provide highly reproducible quantitative maps in both 2D (14) and 3D (15) acquisitions. MRF-derived T_1 and T_2 measurements are also repeatable over time (16), with excellent reproducibility *in vivo* across different scanner types (17,18). Several *in vivo* multicenter studies demonstrated high levels of repeatability and reproducibility of MRF in the brain (17,19). However, repeatability and reproducibility of the prostate MRF acquisition in phantom and prostatic tissues across different centers has not yet been demonstrated.

The purpose of this study was to evaluate multicenter repeatability and reproducibility of T_1 and T_2 estimates based on the MRF technique using the International Society for Magnetic Resonance in Medicine/National Institute of Standards and Technology (ISMRM/NIST) MRI system phantom (20) and prostatic tissues in patients.

METHODS

MRF Data Acquisition

This HIPAA compliant study was approved by the local Institutional Review Board (IRB), and written informed consent was obtained for all *in vivo* scans. Experiments were performed on five different 3T MRI scanners (one Skyra and four Verio scanners, Siemens Healthcare, Erlangen, Germany) with different software versions (VE11C, VB19, and VB17) in three different institutions: University Hospitals Cleveland Medical Center (UHCMC) and Brigham and Women's Hospital (BWH) in the United States, and Diagnosticos da America (DASA) in Brazil. An MRF-FISP acquisition designed for use in the prostate (21) was employed with the following parameters: FOV 400x400mm^2; matrix 400x400; flip angles 3.38-50°; TR 11.2-14.2ms; slice thickness 5mm; 3000 TRs, acquisition time 39 s/slice. A delay time of 5 seconds was inserted between measurements to ensure sufficient magnetization recovery before beginning the next experiment for both phantom and *in vivo* studies.

MRF Dictionary Simulation

In order to efficiently match each measured signal timecourse to the appropriate combination of tissue property values, a pre-calculated MRF dictionary which can be used as a look-up table was generated using Bloch equation simulations in MATLAB (MathWorks 2015b, Natick, MA). In the prostate region, the T_1 is expected to range between 1000 and 2500 ms, and the T_2 between 20 and 300 ms for 3T systems (8,22,23). Dictionary resolutions of T_1 values of [10:5:90, 100:10:1000, 1020:20:1500, 1550:50:2050, 2150:100:2950] and T_2 values of [2:2:10, 15:5:150, 160:10:200, 250:50:500], denoted by min:step:max (ms), were used to balance between matching accuracy and MRF dictionary size. The dictionary had a total of 5,970 entries.

MRF Map Reconstruction

All map reconstruction was performed using a Gadgetron MRF implementation (24), which was exported from UHCMC to BWH and DASA for on-line reconstruction at

each of the institutions. The computers used to perform the reconstructions had an 8GB Nvidia GeForce GTX 1080 graphics card; a 10 core, 2.2GHz Intel Xeon E5-2630 v4 processor; and 64GB of 2400MHz DDR4 RAM. The raw data was passed to the Gadgetron MRF reconstruction pipeline and processed using PCA-based coil compression to reduce the number of coils from 8-12 to 8, as suggested in (25). To further reduce the computational load and memory requirements without reducing the performance, singular value decomposition (SVD) basis compression (26) was applied to the MRF data to compress the number of time points from 3000 to 43, which preserved 99.9% of collected information. The GPU-enabled NUFFT (27) was then used to grid the data. Multi-coil images were combined with adaptive coil combination (28). Finally, cross-correlation pattern matching was applied to the data using the pre-calculated dictionary to extract quantitative T_1 and T_2 values for each voxel. The Gadgetron reconstruction took 17.8 seconds for each slice.

Phantom Study

The accuracy of the T_1 and T_2 values measured using MRF was validated using the T_2 layer of ISMRM/NIST MRI system phantom with T_1 values between 307.7 and 2360ms and T_2 values between 19.1 and 248.5ms. The phantom was placed in the magnet for at least 20 minutes before the acquisition to reduce any errors due to motion of the water making up the phantom. Six single-slice MRF measurements were then collected, with a delay of 5 seconds between measurements, on all five scanners. Following this acquisition, data for the same-day test-retest study were collected on the UHCMC Verio 1, UHCMC Verio 2, UHCMC Skyra, and DASA Verio. The phantom was moved out of the magnet and placed again in the magnet, again allowed to settle for at least 20 minutes, and another set of six single-slice MRF acquisitions was collected. Neither B_0 nor B_1 maps were collected in this study. The results from the MRF measurements were compared to the reference values measured and reported by NIST (16).

In vivo Prostate Study

In addition to the phantom study, *in vivo* experiments were performed in 24 patients with suspected prostate cancer (seven patients on the UHCMC Verio 1, mean age 68.4 years, age range 67–71 years; six patients on the BWH Verio, mean age 67.3 years, age range 59–76 years; and eleven patients on the DASA Verio, mean age 60.7 years, age range 37–71 years). The protocol used was the same as that described for the phantom study, with the following exceptions. No settling time was required for the *in vivo* prostate measurements, and instead of single-slice measurements, two sets of two-slice MRF measurements with no slice gaps were acquired to assess same-day test-retest reliability. The patients were removed from the scanner and then repositioned between the two MRF acquisitions.

Statistical Analysis

For the ISMRM/NIST MRI system phantom study, the mean and standard deviation (SD) for each sphere was calculated from a circular region of interest (ROI, 70 pixels in size with a radius of 4.7mm) that was manually drawn on the maps. For repeatability, intra-scanner variation of T_1 and T_2 values was assessed using the coefficient of variation (CV), defined as the ratio of the standard deviation to the mean of six measurements and expressed as a percentage:

$$CV_{intra-scanner} = 100 \times \frac{SD\ of\ 6\ measurements}{mean\ of\ 6\ measurements}.$$

The intra-scanner variation was calculated for each MRI scanner. For reproducibility, the coefficient of variation for T_1 and T_2 values between the four clinical scanners was calculated to demonstrate inter-scanner variation:

$$CV_{inter-scanner} = 100 \times \frac{SD\ of\ measurements\ from\ 4\ scanners}{mean\ of\ measurements\ from\ 4\ scanners}.$$

The mean of all six measurements was first calculated for each scanner. The mean and standard deviation across the four scanners were then calculated and compared to the mean and standard deviation for measurement #5 to show the differences between inter-scanner variation from multiple measurements and a single measurement.

For the *in vivo* subjects, ROIs in the peripheral zone (PZ) and transitional zone (TZ) were drawn by a radiologist (L.K.B., with 13 years of radiology experience) in maps from

both scans for all patients. Note that the ROIs from patients (10 pixels in size) were drawn in normal appearing regions (PI-RADS 1 or PI-RADS 2) with no specific findings. Mean T_1 and T_2 values were calculated for each ROI. The intra-class correlation coefficient (ICC(3,1)) and Bland-Altman analysis were used to evaluate the test-retest reliability in the *in vivo* prostate study.

RESULTS

The means of the six measurements obtained from the ISMRM/NIST MRI system phantom on five scanners at the three different medical institutions are presented in Figure 1. The x-axis labels are the reference values for each of the spheres as measured and reported by NIST. The results show a strong linear correlation ($R^2 > 0.998$ for T_1, $R^2 > 0.994$ for T_2) with the reference values. The bias for each vial (calculated as the difference between the measured T_1 and T_2 values and the reference values, divided by the reference values) for each of the five scanners is shown in Supporting Information Figure S1.

Figure 2 shows the CV for each of the spheres with T_1 values between 307.7 and 2360.0ms and T_2 values between 19.1 and 248.5ms, as calculated by dividing the standard deviation of the six repeat measurements by the mean of the six measurements (expressed as a percentage). Figures 2a and 2b show the intra-scanner CVs for T_1 and T_2. The T_1 estimates had a variation of 0.2% to 2.0% and T_2 estimates had a variation of 0.0% to 4.7%, with the exception of the vial with a T_2 value of 19.1ms, which showed a variation of 8.9%. The inter-scanner CVs over all six measurements are shown in orange in Figure 2c and 2d, and the CVs for a single measurement (#5 of the six measurements) are shown in blue. These inter-scanner measurements exhibited a T_1 variation of 2.3% to 4.9% for T_1 values between 307.7 and 2360.0ms and T_2 variation of 2.3% to 8.1% for T_2 values between 40.5 and 248.5ms. The variation increased in spheres with T_2 values of lower than 28.8ms. The difference between inter-scanner variations of multiple measurements and the variation in a single measurement is less than 2%.

The test-retest reliability coefficients for both T_1 and T_2 values in the ISMRM/NIST MRI system phantom were above 0.99 between repeated measurements made on the

UHCMC Verio 1, UHCMC Verio 2, UHCMC Skyra, and DASA Verio (Figure 3 and Supporting Information Figure S2).

Supporting Information Figure S3 shows representative prostate MRF T_1 and T_2 maps in patients from five different scanners. For the same-day test-retest *in vivo* prostate experiments performed on patients, the mean T_1 and T_2 values in both the peripheral zone and transition zones are shown in Figure 4a-4d. The mean and standard deviation of T_1 and T_2 values in these zones are given in Table 1. The test-retest reliability coefficients demonstrate test-retest reliability ICC > 0.92 in both prostate regions at all three sites.

The Bland-Altman analysis revealed that 24 of 24 PZ T_1 measurements, 22 of 24 PZ T_2 and TZ T_1 measurements, and 23 of 24 TZ T_2 measurements fell within the 95% confidence interval (CI) for limits of agreement, when difference in measurements was plotted against the mean of the measurements (Figure 4). The T_1 values obtained from PZ and TZ demonstrated a strong linear correlation (R^2 = 0.978 and R^2 = 0.936, respectively) and acceptable agreement (bias 41.1ms, 95% CI -74.3ms to 156.6ms; bias 15.2ms, 95% CI -90.7ms to 121.1ms). The T_2 values from PZ and TZ also showed a strong linear correlation (R^2 = 0.840 and R^2 = 0.970, respectively) and acceptable agreement (bias 4.5ms, 95% CI -41.8ms to 56.7ms; bias -0.45ms, 95% CI -13.4ms to 12.5ms) with corresponding plots presented in Figure 4f and 4h, respectively.

DISCUSSION

This study assesses the repeatability and reproducibility of prostate MRF derived T_1 and T_2 measurements on five different 3T MRI scanners with different software versions in three different medical institutions. It also demonstrates the use of a Gadgetron-based online MRF reconstruction to generate quantitative maps rapidly at the scanner. This implementation enabled the same MRF reconstruction to be used on five different MRI scanners in three different locations, where the personnel had technical expertise ranging from minimal to advanced. Additionally, the improvement in the workflow made possible through the use of the online reconstruction meant that

quantitative maps could be provided immediately to the radiologist for annotation and analysis. Coupled with the results demonstrating repeatability and reproducibility, this work paves the way for a Gadgetron-based MRF framework for quantitative mapping of the prostate to be distributed and used at a variety of MRI scanners around the world.

This study reports the repeatability and reproducibility of prostate MRF performed at different centers on different continents. Over the wide ranges of T_1 and T_2 values found in the ISMRM/NIST system phantom, intra-scanner MRF T_1 and T_2 estimates showed small variations over six measurements. The inter-scanner measurements showed larger T_1 and T_2 variations between scanners at different institutions, which is similar to the results reported in (19). These measurements are in-line with other quantitative measurements in the prostate; previous research has shown that the repeatability CV for measurements of ADC in the prostate is < 2.4% and reproducibility CV is < 4.0% across three 3T scanners (29). Our findings of repeatability (T_1 CV < 2.0% and T_2 CV < 4.7%) and reproducibility (T_1 CV < 4.9% and T_2 CV < 8.1%) for MRF T_1 and T_2 values in the phantom are similar to the reported prostate ADC values. However, T_2 values lower than 30ms and higher than 300ms demonstrated larger variation. An underestimation of very high T_2 values (> 300 ms) in the phantom study was observed as compared to reference values in Figure 1, but variations in this range of T_2 are not expected to be clinically relevant in the prostate as cancer and prostatitis have much shorter measured T_2. The T_2 step size in the MRF dictionary was set to 10ms from 160 to 200ms and 50ms from 250 to 500ms, as such high values were not originally expected to be encountered *in vivo*. Finer dictionary step size and higher maximum T_2 values in the dictionary may improve the accuracy of high T_2 values. Similarly, the higher CV seen for vials with a T_2 value below 30ms likely relates to dictionary coarseness (5ms at this range), which is a substantial fraction of the measured values. A finer dictionary with smaller step sizes could result in an improved test-retest agreement and a lower CV. Other factors that may increase systematic variation of the measured T_1 and T_2 values (Figure S1 and S2) include temperature, B_0 inhomogeneity, and B_1 inhomogeneity.

In addition to the phantom experiment, this study also examined *in vivo* measurements in prostatic tissues. The phantom study demonstrated same-scanner test-retest reliability ICC > 0.99, while the *in vivo* study showed test-retest reliability ICC > 0.92. The slightly lower agreement in the *in vivo* study as compared to the phantom is likely due to a combination of patient motion, physiologic differences, dictionary coarseness, partial volume effects, and B_0 field drift. Because the test-retest scans were performed after moving the subject, the slice selected may also be slightly different, and this could add further variation to the values measured. Partial volume effects could affect the measurements, especially if evaluating small structures/lesions and smaller glands. Thinner slices with a higher spatial resolution would improve the partial volume effects in subjects with small prostates. Main magnetic field drifts could cause errors in T_2 values. The same center frequency was used for all scans in single experiment. Adjusting center frequency before each scan may improve the reproducibility.

Differences were observed between the average T_1 and T_2 values of the peripheral zone in the three measurements from different institutions. The patient data collected from BWH showed lower T_1 and T_2 values as compared to the normal peripheral zone and higher T_1 and T_2 values as compared to prostate cancer and non-cancers reported in literature (7). The differences between groups likely related to differences in populations from which these cohorts were drawn. Some of the patients from BHW underwent prior biopsy or brachytherapy before MRF measurement and may have different tissue properties as compared to other two sites. Several patients had small or almost no PI-RADS 1 peripheral zone due to either prior therapy or due to benign prostatic hypertrophy (PI-RADS 2 with no specific findings), and thus peripheral zone measurements in these patients were difficult to obtain and may contain significant partial volume effects. Finally, small cohorts were scanned due to workflow pressures and distances between sites, and thus patients at each site were not from homogeneous populations. For these reasons, while exact matched comparisons between the patients at the three sites were not possible for this early study, studies with closely matched patient populations can be explored in the future.

One of the limitations in this work was the lack of age-matched healthy subjects. However, the focus of this study was on repeatability and reproducibility and not to provide normative ranges for T_1 and T_2 in the prostate. In order to extend the MRF results to the general population as imaging biomarkers of disease status, repeatability and reproducibility could be assessed in larger populations that include age-matched healthy subjects and patients with different pathologies.

CONCLUSION

MRF measurements of T_1 and T_2 using the FISP-MRF prostate protocol are highly repeatable and reproducible between MRI scanners at different centers on different continents.

REFERENCES

1. Ma D, Gulani V, Seiberlich N, et al. Magnetic resonance fingerprinting. Nature 2013;495:187–92 doi: 10.1038/nature11971.

2. Yu AC, Badve C, Ponsky LE, et al. Development of a Combined MR Fingerprinting and Diffusion Examination for Prostate Cancer. Radiology 2017;283:729–738 doi: 10.1148/radiol.2017161599.

3. Chen Y, Jiang Y, Pahwa S, et al. MR Fingerprinting for Rapid Quantitative Abdominal Imaging. Radiology 2016;279:278–286 doi: 10.1148/radiol.2016152037.

4. Hamilton JI, Jiang Y, Chen Y, et al. MR fingerprinting for rapid quantification of myocardial T1, T2, and proton spin density. Magn. Reson. Med. 2017;77:C1 doi: 10.1002/mrm.26668.

5. Badve C, Yu A, Dastmalchian S, et al. Magnetic Resonance Fingerprinting of Adult Brain Tumors: Initial Experience. AJNR Am Neuroradiol. 2016;51:87–100 doi: 10.1037/a0038432.Latino.

6. European Society of Radiology (ESR). Magnetic Resonance Fingerprinting - a promising new approach to obtain standardized imaging biomarkers from MRI. Insights Imaging 2015;6:163–165 doi: 10.1007/s13244-015-0403-3.

7. Panda A, O'Connor G, Lo WC, et al. Targeted Biopsy Validation of Peripheral Zone Prostate Cancer Characterization With Magnetic Resonance Fingerprinting and Diffusion Mapping. Invest. Radiol. 2019:1 doi: 10.1097/rli.0000000000000569.

8. Panda A, Verena O, W.-C. L, et al. MR Fingerprinting and ADC Mapping for Characterization of Lesions in Transition Zone of the Prostate Gland. Radiology.

9. Panda A, Mehta BB, Coppo S, et al. Magnetic Resonance Fingerprinting-An Overview. Curr. Opin. Biomed. Eng. 2017;3:56–66 doi: 10.1016/j.cobme.2017.11.001.

10. Hsieh JJL, Svalbe I. Magnetic resonance fingerprinting: from evolution to clinical applications. J. Med. Radiat. Sci. 2020;67:333–344 doi: 10.1002/jmrs.413.

11. Ropella-Panagis KM, Seiberlich N, Gulani V. Magnetic Resonance Fingerprinting: Implications and Opportunities for PET/MR. IEEE Trans. Radiat. plasma Med. Sci. 2019;3:388–399 doi: 10.1109/trpms.2019.2897425.

12. Sushentsev N, Kaggie JD, Buonincontri G, et al. The effect of gadolinium-based contrast agent administration on magnetic resonance fingerprinting-based T(1) relaxometry in patients with prostate cancer. Sci. Rep. 2020;10:20475 doi: 10.1038/s41598-020-77331-4.

13. Warntjes JBM, Engström M, Tisell A, Lundberg P. Brain Characterization Using Normalized Quantitative Magnetic Resonance Imaging. PLoS One 2013;8 doi: 10.1371/journal.pone.0070864.

14. Ma D, Coppo S, Chen Y, et al. Slice profile and B1corrections in 2D magnetic resonance fingerprinting. Magn. Reson. Med. 2017;78:1781–1789 doi: 10.1002/mrm.26580.

15. Ma D, Jiang Y, Chen Y, et al. Fast 3D magnetic resonance fingerprinting for a whole-brain coverage. Magn. Reson. Med. 2018;79:2190–2197 doi: 10.1002/mrm.26886.

16. Jiang Y, Ma D, Keenan KE, Stupic KF, Gulani V, Griswold MA. Repeatability of magnetic resonance fingerprinting T1 and T2 estimates assessed using the ISMRM/NIST MRI system phantom. Magn. Reson. Med. 2016 doi: 10.1002/mrm.26509.

17. Körzdörfer G, Kirsch R, Liu K, et al. Reproducibility and Repeatability of MR Fingerprinting Relaxometry in the Human Brain. Radiology 2019;292:429–437 doi: 10.1148/radiol.2019182360.

18. Sushentsev N, Kaggie JD, Slough RA, Carmo B, Barrett T. Reproducibility of magnetic resonance fingerprinting-based T1 mapping of the healthy prostate at 1.5 and 3.0 T: A proof-of-concept study. PLoS One 2021;16:e0245970 doi: 10.1371/journal.pone.0245970.

19. Buonincontri G, Biagi L, Retico A, et al. Multi-site repeatability and reproducibility of MR fingerprinting of the healthy brain at 1.5 and 3.0 T. Neuroimage 2019;195:362–372 doi: 10.1016/j.neuroimage.2019.03.047.

20. Stupic KF, Ainslie M, Boss MA, et al. A standard system phantom for magnetic resonance imaging. Magn. Reson. Med. 2021;86:1194–1211 doi: https://doi.org/10.1002/mrm.28779.

21. Jiang Y, Ma D, Seiberlich N, Gulani V, Griswold MA. MR fingerprinting using fast

imaging with steady state precession (FISP) with spiral readout. Magn. Reson. Med. 2015;74:1621–1631 doi: 10.1002/mrm.25559.

22. Simpkin CJ, Morgan VA, Giles SL, Riches SF, Parker C, deSouza NM. Relationship between T2 relaxation and apparent diffusion coefficient in malignant and non-malignant prostate regions and the effect of peripheral zone fractional volume. Br. J. Radiol. 2013;86:20120469 doi: 10.1259/bjr.20120469.

23. Baur ADJ, Hansen CM, Rogasch J, et al. Evaluation of T1 relaxation time in prostate cancer and benign prostate tissue using a Modified Look-Locker inversion recovery sequence. Sci. Rep. 2020;10:3121 doi: 10.1038/s41598-020-59942-z.

24. Lo W-C, Jiang Y, Franson D, Griswold M, Gulani V, Seiberlich N. MR Fingerprinting using a Gadgetron-based reconstruction. Proc. ISMRM Work. MRF, Cleveland, OH 2017.

25. Hansen MS, Sørensen TS. Gadgetron: An open source framework for medical image reconstruction. Magn. Reson. Med. 2013;69:1768–1776 doi: 10.1002/mrm.24389.

26. McGivney DF, Pierre E, Ma D, et al. SVD compression for magnetic resonance fingerprinting in the time domain. IEEE Trans. Med. Imaging 2014;33:2311–2322 doi: 10.1109/TMI.2014.2337321.

27. Sorensen TS, Schaeffter T, Noe KO, Hansen MS. Accelerating the nonequispaced fast fourier transform on commodity graphics hardware. IEEE Trans. Med. Imaging 2008;27:538–547 doi: 10.1109/TMI.2007.909834.

28. Inati SJ, Hansen MS, Kellman P. A Solution to the Phase Problem in Adaptive Coil Combination. Proc. 21th Annu. Meet. ISMRM, Salt Lake City, UT. 2013:Abstract #2672.

29. Wang Y, Tadimalla S, Rai R, et al. Quantitative MRI: Defining repeatability, reproducibility and accuracy for prostate cancer imaging biomarker development. Magn. Reson. Imaging 2021;77:169–179 doi: 10.1016/j.mri.2020.12.018.

Table 1. The mean and standard deviation (SD) of T_1 and T_2 values and same-day test-retest reliability of measurements in prostatic tissue in patients in the peripheral zone (PZ) and transition zone (TZ).

			UHCMC Verio 1		BWH Verio		DASA Verio	
			7 Patients (68.4±1.4 yrs)		6 Patients (67.3±6.2 yrs)		11 Patients (60.7±9.0 yrs)	
			Mean±SD (ms)	ICC (95% CI)	Mean±SD (ms)	ICC (95% CI)	Mean±SD (ms)	ICC (95% CI)
T_1	PZ	test	2551.8±409.7	0.99 (0.98-1.00)	2153.4±331.1	0.99 (0.92-1.00)	2257.6±378.9	0.98 (0.88-1.00)
		retest	2471.9±407.4		2136.6±317.9		2150.6±546.1	
	TZ	test	1880.0±233.3	0.96 (0.87-0.99)	1773.8±244.1	0.94 (0.70-0.99)	1740.7±166.0	1.00 (0.98-1.00)
		retest	1827.6±194.3		1778.8±246.2		1738.2±156.2	
T_2	PZ	test	164.1±73.9	0.94 (0.78-0.98)	115.4±48.7	0.92 (0.59-0.99)	146.0±59.4	0.94 (0.63-0.99)
		retest	136.1±55.5		122.3±38.4		143.7±58.8	
	TZ	test	77.6±54.0	0.98 (0.92-0.99)	76.7±40.9	1.00 (0.99-1.00)	69.3±18.5	0.98 (0.89-1.00)
		retest	72.6±52.0		83.1±48.8		70.0±18.1	

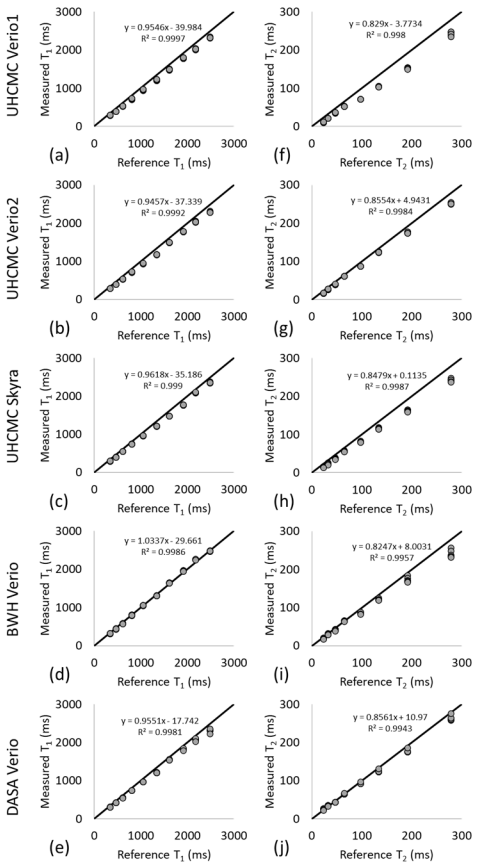

MRM_29264_Figure1.tiff

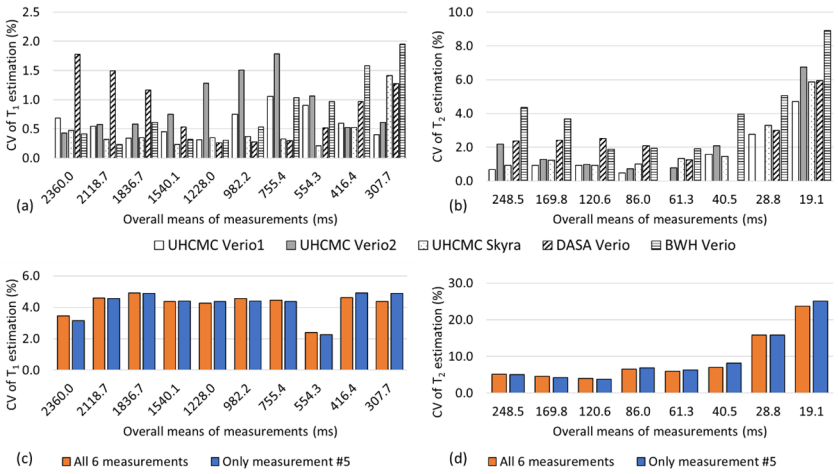

MRM_29264_Figure2.tiff

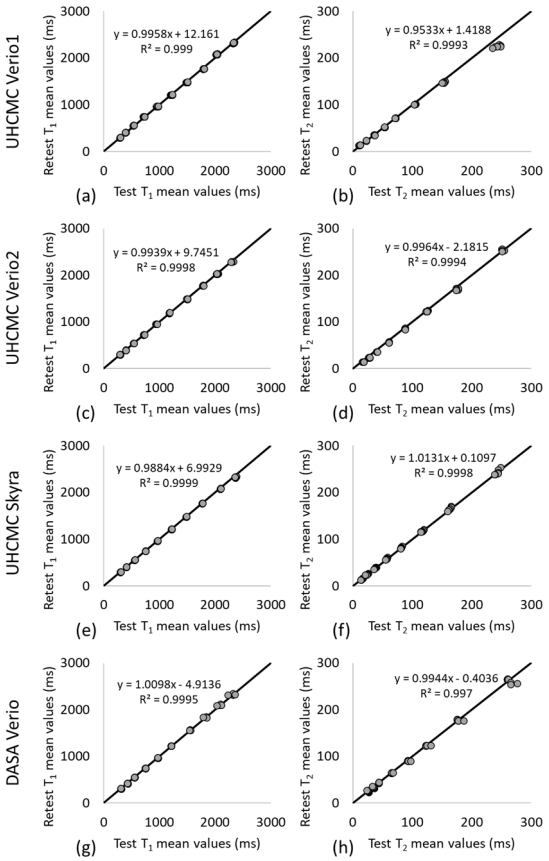

MRM_29264_Figure3.tiff

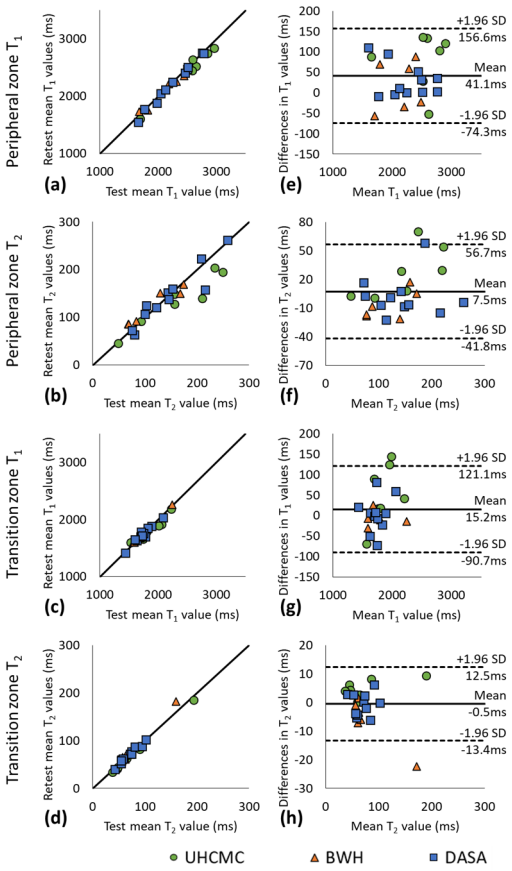

MRM_29264_Figure4.tiff